Controlled wave-function mixing in strongly coupled one-dimensional wires

K. J. Thomas, J. T. Nicholls, M. Y. Simmons, W. R. Tribe, A. G. Davies, and M. Pepper
Cavendish Laboratory, Madingley Road, Cambridge CB3 0HE, United Kingdom
(Received 30 September 1998)

We investigate the transport properties of two strongly coupled ballistic one-dimensional (1D) wires, defined by a split-gate structure deposited on a GaAs/AlGaAs double quantum well. Matching the widths and electron densities of the two wires brings them into resonance, forming symmetric and antisymmetric 1D subbands separated by energy gaps that are measured to be larger than their two-dimensional counterparts. Applying a magnetic field parallel to the wire axes enhances wave-function mixing at low fields, whereas at high fields the wires become completely decoupled. [S0163-1829(99)07315-4]

The energy levels of a two-level system described by a Hamiltonian $H(a)$ may cross at some particular value of the parameter a. A perturbation applied to the system will couple the two levels, which will repel each other in accordance with the ''no-crossing'' theorem.[1] For example, a pair of near-degenerate Stark levels in the spectrum of a Rydberg atom in an electric field can be considered to be such a two-level system.[2] In this paper we show that similar behavior can be observed in a mesoscopic system when the energy levels of two ballistic one-dimensional (1D) wires are brought together. When the wires have equal width and density, the symmetry of the 1D wave functions allow the interwire interaction (the perturbation) only to couple subbands of the same index, giving rise to symmetric and antisymmetric wave functions. The gate voltages controlling the device play the role of the parameter a, and an in-plane magnetic field (either parallel $B_{\|}$ or perpendicular $B_{\perp}$ to the wire axes) can tune the interwire interaction.

The transport properties of a single ballistic 1D constriction, defined by a split-gate deposited over a high-mobility two-dimensional electron gas (2DEG), are well known.[3] As the voltage applied to the split gate (V_{sg}) is made more negative the 1D subbands are depopulated, and the conductance drops by $2e^2/h$ as each spin-degenerate subband passes through the chemical potential. By fabricating[4] a modified split gate over a double quantum well sample, the two ballistic 1D constrictions (2×1D) can be brought together, one on top of the other (see Fig. 1, inset). The wafer (T210), grown by molecular-beam epitaxy, comprises two 150-Å-wide GaAs quantum wells separated by a 25-Å $Al_{0.33}Ga_{0.67}As$ barrier, with a center-to-center distance of $d=175$ Å. The double quantum well is doped both above and below using 2000 Å of Si-doped (1.2×10^{17} cm^{-3}) $Al_{0.33}Ga_{0.67}As$, offset by 600 Å and 800 Å $Al_{0.33}Ga_{0.67}As$ spacer layers, respectively. The carrier density in each layer is 1.3×10^{11} cm^{-2}, with an average mobility of 1.45×10^6 cm^2/V s. The 2D symmetric-antisymmetric (SAS) energy gap at resonance was measured[5] to be $\Delta_{SAS}=1.4$ meV. The wafer was processed into a Hall bar with Ohmic contacts which connect to both 2DEGs, and the gate pattern shown in the Fig. 1 inset was defined by electron beam lithography. The split-gate has a width of 1.2 μm and a length of 0.4 μm, and to add further control, a midline gate of width 0.4 μm was deposited along the center of the split gate. Our previous measurements[4] of ballistic 2×1D devices show two results: When the barrier separating the two 2DEG's is 300 Å wide, $\Delta_{SAS}\approx0$, and the two 1D wires behave independently with conductances that add. In a 35-Å barrier sample the coupling is stronger ($\Delta_{SAS}\approx1$ meV), and there is mixing of the 1D subbands. In this paper we have been able to index the coupled subbands in a similar sample, and show that their behavior in zero and finite in-plane magnetic field can be described by a simple model.

The two-terminal conductance $G=dI/dV$ of the parallel wires was measured at dilution fridge temperatures using standard techniques.[6] Conductance traces $G(V_{sg})$ of the 2×1D device are shown in Fig. 1, as the midline voltage V_{mid} was changed from 0.16 to -1.0 V in 40-mV steps. After correcting for a series resistance, $R_s=550$ Ω, the plateaus in the conductance are quantized in units of $2e^2/h$. The split-gate voltage V_{sg} defines both the upper (u) and lower (l)

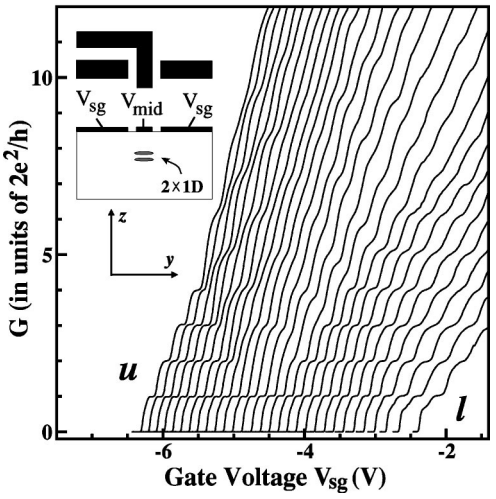

FIG. 1. Conductance characteristics $G(V_{sg})$ at 1.65 K, where from left to right V_{mid} is decreased from 0.16 to -1.0 V in steps of 40 mV. In the region to the left (right), only the upper (lower) wire is occupied. Inset: Schematic plan and side view of the device. The 2×1D electron gases are formed 2800 Å below the sample surface; they lie parallel to the x axis (out of the page), coupled in the z direction, with lateral confinement in the y direction provided by the split gate.

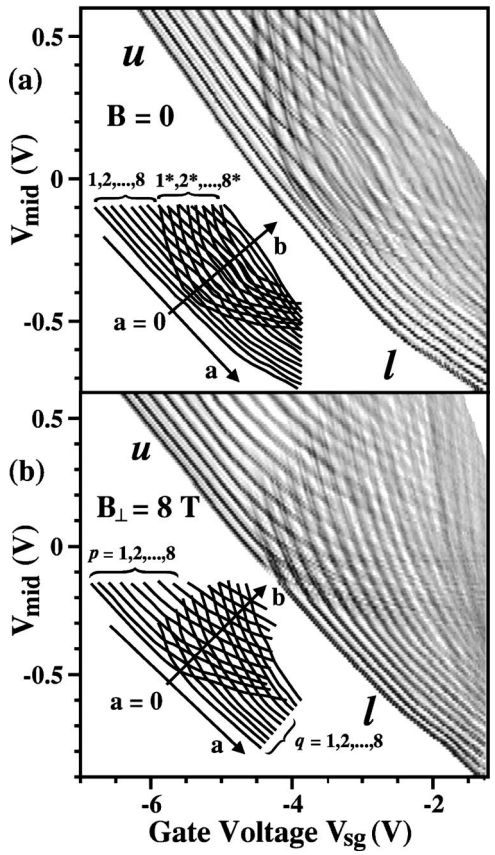

FIG. 2. Transconductance (dG/dV_{sg}) data at 60 mK presented as a gray-scale plot at (a) $B=0$ and (b) $B_{\perp}=8$ T. The insets show the indexed subbands plotted with new axes (a,b).

wires; however, as V_{sg} becomes more negative measurements show[4] that the subbands in the l wire are depopulated first. The midline voltage V_{mid} has the opposite effect; as it is made more negative the u wire is depopulated first. Therefore, by varying V_{sg} and V_{mid}, the fraction of the current passing through the u and l wires can be tuned. The clean conductance steps on the left-hand and right-hand sides of Fig. 1 originate from conduction through just the u and l wires, respectively. The more complicated structure in between occurs where 1D subbands of the two wires become nearly degenerate.

To understand the conductance characteristics better, they are differentiated[4] with respect to V_{sg} to generate the gray-scale plot[7] in Fig. 2(a). The dark lines denote the transconductance (dG/dV_{sg}) maxima between plateaus, indicating where a 1D subband edge passes through the chemical potential. The Fig. 2(a) inset shows the subband positions redrawn with new axes (a, b) and indexed by n and n^*, which are (to be shown later) the bonding and antibonding states formed by mixing the nth wave functions of the u and l wires.

A magnetic field B applied parallel to the two 2DEG's shifts the Fermi circles (of radii $k_{F,u}$ and $k_{F,l}$) with respect to each other by $\Delta k=eBd/\hbar$.[8] The Fermi circles are completely decoupled when $\Delta k>k_{F,u}+k_{F,l}$, which for the carrier densities in our sample occurs for $B>7$ T. Figure 2(b) shows dG/dV_{sg} in an in-plane field $B_{\perp}=8$ T. A similar plot is obtained for $B_{\parallel}=8$ T, and for both field directions the characteristics are similar to those observed[4] when the u and l wires are decoupled in a 300-Å barrier sample. The subbands in Fig. 2(b) are indexed with integers p and q, corresponding to the quantization of the conductance (in units of $2e^2/h$) in the u and l wires. In Fig. 2(b) decoupled subbands of the same index cross without mixing at $a=0$, the same line along which there are anticrossings between the n and n^* subbands at $B=0$ [Fig. 2(a)]. In addition to this decoupling at $B=8$ T, there is also evidence of spin-splitting of the 1D subbands.

The potential in a single 1D constriction is well described by a saddle point,[9,10] where there is parabolic confinement in the y direction and a parabolic barrier to free motion in the x direction. The conductance (in units of $2e^2/h$) is determined by the number of occupied 1D subbands at the saddle point. For the 2×1D device we assume that the two saddle points are aligned at the same (x,y) position, and the transport properties are determined by the mixing of the highest occupied wave functions, Ψ_j (where $j=u$ or l), at this point. If separable, the unperturbed wave function in each wire is given by

$$\Psi_j(x,y,z)=e^{ik_x x}\phi_{j,m}(y)Z_{j,m}(z), \tag{1}$$

where $m=p$ for $j=u$, and $m=q$ for $j=l$. $\phi_{j,m}(y)$ is the mth 1D subband wave function, and $Z_{j,m}(z)$ is the ground-state 2D wave function in the quantum well. $Z_{j,m}(z)$ is a function of the carrier density at the saddle point, and hence it depends on the 1D subband index m. For $k_x=0$, there is peak in dG/dV_{sg}, and the matrix element that determines the mixing between the p and q subbands of the u and l wires is

$$\langle\Psi_u|V(z)|\Psi_l\rangle = \int \phi_{u,p}(y)\phi^*_{l,q}(y)dy \int Z_{u,p}(z)V(z)Z^*_{l,q}(z)dz, \tag{2}$$

where $V(z)$ is the conduction-band profile of the double quantum well structure. If the integral

$$I=\int \phi_{u,p}(y)\phi^*_{l,q}(y)dy \tag{3}$$

is zero, then $\langle\Psi_u|V(z)|\Psi_l\rangle=0$, and the p and q 1D subbands cross without mixing. I is determined by both the alignment of the wires and the symmetries of the two 1D wave functions. If misaligned, then in general $I\neq0$, and there will be complicated mixing between all subbands of the two wires; this is not observed in the $B=0$ results shown in Fig. 2(a), supporting the assumption that the two saddle points are approximately aligned. For aligned wires, $I=\delta_{p,q}$, if the wires have the same width. If the wires have different widths $I\neq0$ only when p and q are either both odd or even. Figure 2(a) does not show this odd-even mixing expected for wires of very different widths, and so we believe that the aligned wires have approximately equal widths.[11] In which case the y and z components of the unperturbed wave functions mix when $p=q=n$ to give

$$F_n(y,z)=[\phi_{l,n}(y)Z_{l,n}(z)+\beta\phi_{u,n}(y)Z_{u,n}(z)]/\sqrt{1+\beta^2}, \tag{4}$$

and

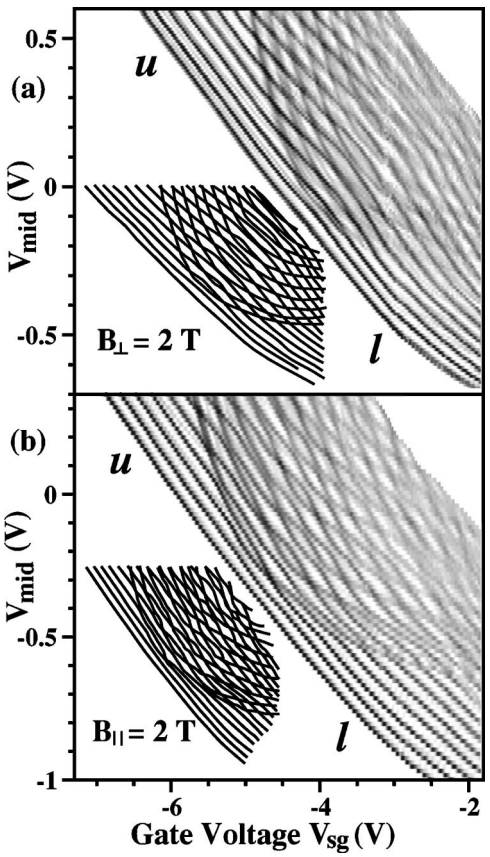

FIG. 3. Gray-scale plots of dG/dV_{sg} as a function of V_{mid} and V_{sg} at (a) $B_{\perp}=2$ T and (b) $B_{\parallel}=2$ T.

$$F_{n*}(y,z)=[\beta\phi_{l,n}(y)Z_{l,n}(z)-\phi_{u,n}(y)Z_{u,n}(z)]/\sqrt{1+\beta^2}. \tag{5}$$

The number β describes how much of the wave function is in each wire and is determined by the position on the a axis, which is itself a linear combination of V_{sg} and V_{mid}. For example, the state labeled $n=1$ in Fig. 2(a) has the wave function $F_1(y,z)$. When a is large and negative, $\beta\rightarrow\infty$, and conduction is through the u wire. When a is large and positive, $\beta\rightarrow 0$, and conduction proceeds through the l wire. At $a=0$ the 1D levels are at resonance ($\beta=1$) and the integral

$$\int Z_{u,n}(z)V(z)Z^{*}_{l,n}(z)dz=\Delta^{n}_{SAS}/2, \tag{6}$$

defines the energy gap Δ^{n}_{SAS} between the symmetric and antisymmetric 1D subbands at their anticrossing. Going along the b axis increases the number of occupied 1D subbands. For example in Fig. 2(a), at $a=0$ the symmetric and antisymmetric subbands are populated in the order 1,2,1*,3,2*, ... For this reason the gray scale plots can be thought of as ''energy'' diagrams $E_b(a)$.

At $B=0$ the integral $I=\delta_{p,q}$, and there is only mixing between subbands of the same index. Using an in-plane field of $B=2$ T, we can alter I so that there is also mixing between subbands of different index; though, unlike the high field case ($B>7$ T), the energy diagram $E_b(a)$ is sensitive to the direction of the in-plane field. When $B_{\perp}=2$ T, see Fig. 3(a), $E_b(a)$ is similar to that obtained at $B=0$ [Fig. 2(a)], and there is no evidence of new anticrossings. In contrast, for

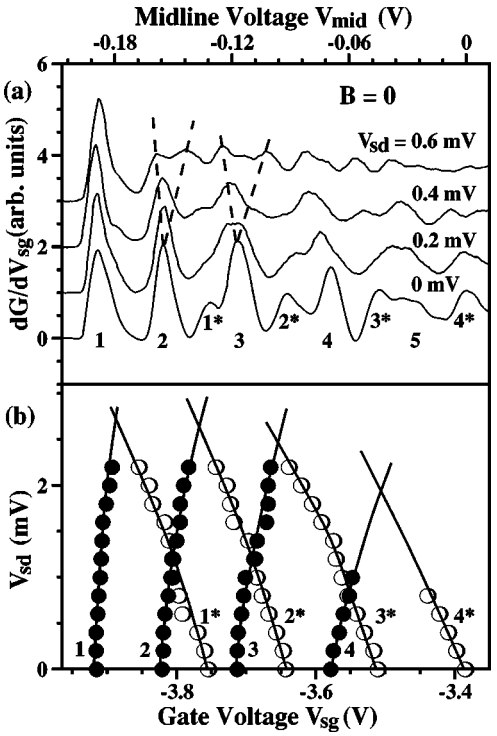

FIG. 4. (a) Traces of dG/dV_{sg} on resonance ($a=0$) at $V_{sd}=0$, 0.2, 0.4, and 0.6 mV, obtained along the b axis, a linear combination of V_{mid} and V_{sg}, which are swept simultaneously across the ranges given at the top and bottom of the figure. (b) The positions of the right-moving transconductance peaks of the n subbands (●), and the left-moving peaks of the n^* subbands (○) as a function of V_{sd}. The solid lines are guides to the eye, showing the crossing voltages used to calculate Δ^{n}_{SAS}.

$B_{\parallel}=2$ T, see Fig. 3(b), there is strong mixing that gives rise to complicated crossings and anticrossings. In a $B_{\parallel}$ field the electron gains momentum $\Delta k_y=eB_{\parallel}d/\hbar$ as it tunnels the distance d in the z direction, and Eq. (3) becomes

$$\begin{aligned} I(B_{\parallel}) &= \int e^{-i\Delta k_y y}\phi_{u,p}(y)\,\phi^{*}_{l,q}(y)dy \\ &= \int \tilde{\phi}_{u,p}(k_y-\Delta k_y)\,\tilde{\phi}^{*}_{l,q}(k_y)dk_y \\ &= \int \tilde{\phi}_{u,p}(k_y-eB_{\parallel}d/\hbar)\,\tilde{\phi}^{*}_{l,q}(k_y)dk_y, \end{aligned} \tag{7}$$

where $\tilde{\phi}_{j,p}(k_y)$ is the Fourier transform of $\phi_{j,p}(y)$. The wave functions of the two wires are shifted with respect to each other in k_y space, and in general $I(B_{\parallel})\neq 0$. The $E_b(a)$ diagram at $B_{\parallel}=1$ T (not shown) exhibits completely different crossings and anticrossings to those at $B_{\parallel}=2$ T [Fig. 3(b)], reflecting the changes in $I(B_{\parallel})$. For the other in-plane direction, $B_{\perp}$, there is no change in k_y and the observed $E_b(a)$ diagrams are nearly identical at low fields, $B_{\perp}\ll 7$ T.

To calibrate the $E_b(a)$ diagrams at $B=0$ we have performed dc source-drain voltage measurements using a spectroscopic technique developed to study single wires.[6] The energy spacing between two subbands is given by the applied dc voltage V_{sd} that causes their split transconductance

(dG/dV_{sg}) peaks to cross. We have used the same technique to measure Δ^n_{SAS}, the energy gap at the n-n^* anticrossings along the b axis at $a=0$. Figure 4(a) shows the dG/dV_{sg} characteristics along the b axis at resonance for $V_{sd}=0$, 0.2, 0.4, and 0.6 mV; V_{sd} doubles the number of dG/dV_{sg} peaks, as shown by dashed lines for $n=2$ and 3. To simplify the picture, Fig. 4(b) shows only the position of the right-moving n peaks and left-moving n^* peaks as a function of V_{sd}. The gap Δ^n_{SAS} is the voltage across the 2×1D device at which adjacent n and n^* peaks cross, and for this reason the crossing voltages measured from Fig. 4(b) are corrected for series resistance effects.[6] The corrected values are $\Delta^n_{SAS}=2.6\pm0.4$, 2.4 ± 0.3, 2.1 ± 0.3, and 1.6 ± 0.3 meV for $n=1$, 2, 3, and 4, respectively. As n increases the Coulomb repulsion associated with the higher carrier density in the vicinity of the constriction pushes the wave functions further apart in the z direction, decreasing the SAS gap towards the 2D limit, $\Delta_{SAS}=1.4$ meV, of the as-grown sample.

We note that the matrix element in Eq. (2) is the same as that used[12] in studies of 1D resonant tunneling diodes, where the tunneling current is proportional to $|\langle\Psi_u|V(z)|\Psi_l\rangle|^2$. In these other studies the anisotropy in the two in-plane field directions was observed, but modeling was required to decide which tunneling transition $n\rightarrow m$ is associated with which structure in the I-V characteristics. For the case of strong coupling considered here, indexing is much easier because the mixing between the u and l subbands is clearly seen in the $E_b(a)$ diagrams, and p and q are determined from the quantized conductance. Other studies[13] have investigated 2×1D wires defined over parabolic quantum wells, but because of the large well width, these systems show strong diamagnetic shifts in an in-plane B field.

In conclusion, we have observed the bonding and antibonding subbands of coupled 1D wires. At resonance, the wires are aligned and have approximately equal widths, and the gap Δ^n_{SAS} at the anticrossing has been measured. Using a simple single-particle model we can understand the overall behavior of the coupled 1D subbands; there is no evidence for subband locking,[14] where 1D subbands are attracted towards each other. The coupled 1D devices are of interest in furthering studies of the *0.7 structure*—this is a reproducible conductance feature at $0.7(2e^2/h)$ that is observed[3,15] in a clean single 1D wire, in addition to the usual quantized conductance plateaus. In a strong parallel magnetic field the 0.7 structure evolves into a spin-split plateau at e^2/h, suggesting that the zero-field structure at $0.7(2e^2/h)$ arises from many-body interactions where spin is an important ingredient. There are indications of a 0.7 structure in Fig. 1.

We thank the Engineering and Physical Sciences Research Council (U.K.) for supporting this work, and J.T.N. also acknowledges support from EPSRC. We thank Dr. N. J. Appleyard for useful discussions.

[1] E. Merzbacher, in *Quantum Mechanics*, 2nd ed. (Wiley, New York, 1970), pp. 428–429.

[2] J. R. Rubbmark, M. M. Kash, M. G. Littman, and D. Kleppner, Phys. Rev. A **23**, 3107 (1981).

[3] K. J. Thomas, J. T. Nicholls, N. J. Appleyard, M. Pepper, M. Y. Simmons, D. R. Mace, and D. A. Ritchie, Phys. Rev. B **58**, 4846 (1998).

[4] I. M. Castleton, A. G. Davies, A. R. Hamilton, J. E. F. Frost, M. Y. Simmons, D. A. Ritchie, and M. Pepper, Physica B **249-251**, 157 (1998).

[5] A. G. Davies, C. H. W. Barnes, K. R. Zolleis, J. T. Nicholls, M. Y. Simmons, and D. A. Ritchie, Phys. Rev. B **54**, R17 331 (1997).

[6] K. J. Thomas, M. Y. Simmons, J. T. Nicholls, D. R. Mace, M. Pepper, and D. A. Ritchie, Appl. Phys. Lett. **67**, 109 (1995).

[7] The data presented are from the same device but taken on different cool downs; as a result the gate voltage positions shift slightly. The data in Figs. 2–4 were obtained at 60 mK, and impurity features are visible in the gray-scale plots shadowing the subband trajectories.

[8] J. P. Eisenstein, T. J. Gramila, L. N. Pfeiffer, and K. W. West, Phys. Rev. B **44**, 6511 (1991).

[9] H. A. Fertig and B. I. Halperin, Phys. Rev. B **36**, 7969 (1987).

[10] L. Martín-Moreno, J. T. Nicholls, N. K. Patel, and M. Pepper, J. Phys.: Condens. Matter **4**, 1323 (1992).

[11] Strictly speaking, the wires only have equal width at $a=0$, but away from resonance the mixing described by I is extremely weak for $p\neq q$.

[12] N. Mori, P. H. Beton, J. Wang, and L. Eaves, Phys. Rev. B **51**, 1735 (1995).

[13] G. Salis *et al.* (unpublished).

[14] Y. Sun and G. Kirczenow, Phys. Rev. Lett. **72**, 2450 (1994).

[15] K. J. Thomas, J. T. Nicholls, M. Y. Simmons, M. Pepper, D. R. Mace, and D. A. Ritchie, Phys. Rev. Lett. **77**, 135 (1996).